SM98
Proceedings of SECTAM-XX
April 16-18, 2000, Callaway Gardens, GA

COMPLEX WAVE-NUMBER DISPERSION ANALYSIS OF STABILIZED FINITE ELEMENT METHODS FOR ACOUSTIC FLUID – STRUCTURE INTERACTION

Lonny L. Thompson, Sridhar Sankar, and Yuhuan Tong
Department of Mechanical Engineering
Clemson University
Clemson, South Carolina, 29634
Email: lonny.thompson@ces.clemson.edu

ABSTRACT

The application of nite element methods to problems in structural acoustics (the vibration of an elastic body coupled to an acoustic medium) is considered. New stabilized methods based on the Hellinger-Reissner variational principle with a generalized least-squares modi cation are developed which yield improvement in accuracy over the standard Galerkin - nite element method for both *in vacuo* and acoustic uid-loaded Reissner-Mindlin plates. Through judicious selection of design parameters this formulation provides a consistent framework for enhancing the accuracy of mixed Reissner-Mindlin plate elements that have no shear locking or spurious modes. Combined with Galerkin Least-Squares (GLS) methods for the acoustic uid, the method presents a new framework for accurate modeling of acoustic uid-loaded structures. The technique of complex wave-number dispersion analysis is used to examine the accuracy of the discretized system in the representation of free-waves for uid-loaded plates. Improved methods are designed such that the nite element dispersion relations closely match each branch of the complex wavenumber loci for uid-loaded plates. Comparisons of nite element dispersion relations demonstrate the superiority of the new hybrid least-squares (HLS) plate elements combined with GLS methods for the uid over standard Galerkin and Galerkin Gradient Least-Squares (GGLS) nite element methods.

INTRODUCTION

When modeling the steady-state response of coupled structural acoustics problems, plate and shell elements are needed to accurately represent both propagating, leaky, and evanescent wave types in the solution. In this paper, the stabilized hybrid plate element developed in (Thompson, 1999) is combined with a Galerkin Least-Squares (GLS) treatment of the acoustic region developed in (Thompson, 1995) for accurate response of uid-loaded Reissner-Mindlin plates. The inclusion of shear deformation and rotary inertia effects in this theory is important for high-frequency response for exural waves in plates. The hybrid plate element is based on the Hellinger-Reissner variational principle with a modi catio n consisting of a residuals of the plate equations of motion in a weighted generalized least-squares operator integrated over element interiors. Through judicious selection of the design parameters inherent in the least-squares modi cation, this formulation provides a consistent framework for enhancing the accuracy of mixed Reissner-Mindlin plate elements which have no shear locking or spurious modes.

Weighted residuals of the governing Euler-Lagrange equations in least-squares form were rst used to stabilize the pathologies exhibited by the classical Galerkin method for the numerical solution of advection-diffusion problems (Hughes, 1989). These so-called Galerkin Least-Squares (GLS) stabilized methods have been successfully employed in a wide variety of applications where enhanced stability and accuracy properties are needed. These ideas have since been extended in (Harari, 1992), and (Thompson, 1995) for the GLS nite element solution to the scalar Helmholtz equation governing wave propagation in acoustic uids. In (Thompson, 1995; Harari, et.al., 1996), nite element dispersion analysis was used to select optimal weighting parameters in the least-squares modi cations to the standard Galerkin method, resulting in improved phase accuracy for both two- and three- dimensional problems.

The rst use of residual based methods for static analysis of plate structures can be found in (Hughes, 1988), where symmetric forms of the equilibrium equations were appended to the standard Galerkin equations to improve accuracy. Later, (Grosh, 1996) applied the Galerkin Gradient Least-Squares (GGLS) method of (Franca, 1989) to improve the accuracy of Timoshenko beam elements for steady-state vibration. In (Grosh, 1998), the GGLS Timoshenko beam element is combined with the one-dimensional GLS method of (Harari, 1992) to study acoustic- uid loaded plates. As expected, the combined use of stabilized methods for both the plate and acoustic uid, yielded improved accuracy over standard Galerkin methods. However, the extension of the GGLS formulation to Reissner-Mindlin plate elements based on bi-linear displacement interpolation failed to produce a general 4-node quadrilateral element which is free

from shear locking (Grosh, 1996), limiting the use of this approach for most realistic applications.

In this work, complex-wavenumber dispersion analysis is used to examine the accuracy of free-waves in the HLS plate elements developed in (Thompson, 1999), coupled with optimal GLS methods for the fluid (Thompson, 1995). The use of finite element dispersion analysis for fluid-loaded plate systems was first performed by (Jasti, 1992), where real-valued free waves in Galerkin based plate elements using Kirchoff's theory and Mindlin's theory, coupled with a Galerkin fluid were studied. Later, (Grosh, 1994) extended his work to include imaginary wavenumbers, and helped to clarify the significance of each wavenumber branch. Dispersion analysis provides a tool for predicting the general trends in behaviour of the elements when used to model boundary value problems with fixed boundaries.

REISSNER-MINDLIN PLATE EQUATIONS

Consider a plate of thickness t, defined on the domain Ω_s such that,

$$\Omega_s = \left\{ (x,y,z) \in R^3,\ z \in [-\frac{t}{2},\frac{t}{2}],\ (x,y) \in \Gamma \subset R^2 \right\} \qquad (1)$$

where Γ is a two-dimensional midsurface and z is the coordinate transverse to this plane. Furthermore, loading $q(x,y)$ is restricted to the direction normal to the midsurface defined as $\boldsymbol{e}_z$.

Mindlin's approximate theory for flexural waves in plates includes shear deformation and rotary inertia effects which are important for high-frequency excitation. The deformation at any point is given by the three-dimensional displacement vector defined by the kinematic relation, $\boldsymbol{u} = -z\boldsymbol{\theta}(x,y) + w(x,y)\boldsymbol{e}_z$, where $\boldsymbol{\theta} = (\theta_x, \theta_y)$ denotes the two-dimensional vector of rotations, such that $\boldsymbol{\theta} \perp \boldsymbol{e}_z$. The components θ_x and θ_y are the rotations of the transverse line elements (perpendicular fibers to the midsurface) about the y and x axes respectively. As a consequence of the kinematic assumptions, the in-plane bending strains $(\varepsilon_{xx}, \varepsilon_{yy}, \gamma_{xy})$, are linearly related to curvatures by,

$$\boldsymbol{\kappa} = [\kappa_{xx}\,,\,\kappa_{yy}\,,\,\kappa_{xy}] = [\theta_{x,x}\,,\,\theta_{y,y}\,,\,\theta_{x,y} + \theta_{y,x}] \qquad (2)$$

while the transverse shear strains are defined by the angle between the slope of the midsurface after deformation and the fiber orientation,

$$\boldsymbol{\gamma} = [\gamma_{xz}\,,\,\gamma_{yz}] = [w_{,x} - \theta_x\,,\,w_{,y} - \theta_y] \qquad (3)$$

For a homogeneous plate with linear elastic material properties, the constitutive relation for the bending and twisting moments $\boldsymbol{M} = [M_x\,,\,M_y\,,\,M_{xy}]$ and shear forces $\boldsymbol{Q} = [Q_x\,,\,Q_y]$ is given by, $\boldsymbol{M} = \boldsymbol{D}_b\,\boldsymbol{\kappa}$, and $\boldsymbol{Q} = \boldsymbol{D}_s\,\boldsymbol{\gamma}$, where for isotropy $\boldsymbol{D}_s = D_s\,\boldsymbol{I}$, $D_s = \kappa G t$, and:

$$\boldsymbol{D}_b = D_b \begin{bmatrix} 1 & \nu & 0 \\ \nu & 1 & 0 \\ 0 & 0 & \frac{(1-\nu)}{2} \end{bmatrix}, \qquad D_b = \frac{Et^3}{12(1-\nu^2)} \qquad (4)$$

with Young's modulus E, Poisson's ratio ν, shear modulus G, and κ is a shear correction factor.

For time-harmonic motion, the coupled equations of motion for the Reissner-Mindlin plate are,

$$L_1[\boldsymbol{u}^*, \boldsymbol{\sigma}^*] := Q_{x,x} + Q_{y,y} - m\omega^2 w = q \qquad (5)$$

$$L_{2x}[\boldsymbol{u}^*, \boldsymbol{\sigma}^*] := M_{x,x} + M_{yx,y} - Q_x + \rho I \omega^2 \theta_x = 0 \qquad (6)$$

$$L_{2y}[\boldsymbol{u}^*, \boldsymbol{\sigma}^*] := M_{xy,x} + M_{y,y} - Q_y + \rho I \omega^2 \theta_y = 0 \qquad (7)$$

where $\boldsymbol{u}^* = [w, \theta_x, \theta_y]$, $\boldsymbol{\sigma}^* = [\boldsymbol{M}, \boldsymbol{Q}]$, and $m = \rho t$ is the mass density per unit area, $I = t^3/12$, and ω is the circular frequency measured in rad/sec.

In the absence of an applied load q, the the plate equations of motion admit solutions of the form,

$$\boldsymbol{u}^* = \begin{Bmatrix} A_w \\ A_{\theta_x} \\ A_{\theta_y} \end{Bmatrix} e^{(i\boldsymbol{k}\cdot\boldsymbol{x})} = \begin{Bmatrix} A_w \\ A_\theta \cos\varphi \\ A_\theta \sin\varphi \end{Bmatrix} e^{(ik_x x)} e^{(ik_y y)} \qquad (8)$$

with $i = \sqrt{-1}$ and wavenumber components,

$$\boldsymbol{k} = \begin{Bmatrix} k_x \\ k_y \end{Bmatrix} = k \begin{Bmatrix} \cos\varphi \\ \sin\varphi \end{Bmatrix}, \qquad k = \sqrt{k_x^2 + k_y^2} \qquad (9)$$

Conditions for the allowed waves are obtained by substituting the assumed exponential (8) for $\boldsymbol{u}^*$ into the homogeneous equations of motion. Two independent characteristic equations associated with transverse deflection and rotation result:

$$\begin{bmatrix} D_s k^2 - \rho t\,\omega^2 & -iD_s k \\ iD_s k & D_b k^2 + D_s - \rho I \omega^2 \end{bmatrix} \begin{Bmatrix} A_w \\ A_\theta \end{Bmatrix} = \begin{Bmatrix} 0 \\ 0 \end{Bmatrix} \qquad (10)$$

Nontrivial solutions for the wave amplitudes A_w and A_θ are obtained by setting the determinant of the characteristic matrix to zero. The result is the dispersion relation relating frequency ω to wavenumber k,

$$ak^4 - bk^2 + c = 0 \qquad (11)$$

where a, b, c are frequency dependent parameters. Considered as a function of k^2, solutions to the plate dispersion relation (11)

occur in pairs: $\pm k_1$ and $\pm k_2$. At frequencies below a cut-off frequency, the wavenumber pair $\pm k_1$ occurs as purely real while the pair $\pm k_2$ is purely imaginary. The real wavenumber pair corresponds to propagating waves while the imaginary pair corresponds to evanescent waves characterized by exponential decay. The influence of the evanescent waves are localized near drivers and discontinuities in the plate, e.g., near boundary layers. In (Thompson, 1999) the discrete counterpart to this continuous dispersion relation was used as a tool for the design of improved finite element methods for steady-state vibration of Reissner-Mindlin plates.

HYBRID LEAST SQUARES FORMULATION

In (Thompson, 1999) a new Hybrid Least Squares (HLS) finite element method based on a modified Hellinger-Reissner functional with independent stress and displacement approximations was developed. The Hellinger-Reissner functional is modified by adding weighted differential operators acting on the residuals of the governing equations of motion for the plate written in least-squares form. This approach may be considered an extension of Galerkin Least Squares (GLS) methods to mixed/hybrid methods. The functional given in (Thompson, 1999) can be written as:

$$\begin{aligned}\Pi_{HLS}(\boldsymbol{u}^*,\boldsymbol{\sigma}^*) &= \Pi_H(\boldsymbol{u}^*,\boldsymbol{\sigma}^*) \\ &+\frac{1}{2}\int_{\tilde{\Gamma}}\tau_1\left\{\left(\frac{\partial}{\partial x}\left[L_1-q\right]\right)^2+\left(\frac{\partial}{\partial y}\left[L_1-q\right]\right)^2\right\}d\Gamma \\ &+\frac{1}{2}\int_{\tilde{\Gamma}}\tau_2\left\{\left(\frac{\partial}{\partial x}\left[L_{2x}\right]\right)^2+\left(\frac{\partial}{\partial y}\left[L_{2y}\right]\right)^2\right\}d\Gamma\end{aligned} \tag{12}$$

In the above, $\tilde{\Gamma}=\cup_e\Gamma_e$ is the sum of element interiors Γ_e, and $\Pi_H(\boldsymbol{u}^*,\boldsymbol{\sigma}^*)$ defines the Hellinger-Reissner functional for the plate equations of motion,

$$\begin{aligned}\Pi_H(\boldsymbol{u}^*,\boldsymbol{\sigma}^*) &= \int_\Gamma \boldsymbol{\sigma}^{*T}\boldsymbol{\varepsilon}^*\,d\Gamma-\frac{1}{2}\int_\Gamma \boldsymbol{\sigma}^{*T}\boldsymbol{D}^{-1}\boldsymbol{\sigma}^*\,d\Gamma \\ &-\frac{\omega^2}{2}\int_\Gamma \boldsymbol{u}^{*T}\boldsymbol{C}\boldsymbol{u}^*\,d\Gamma\end{aligned} \tag{13}$$

and,

$$\boldsymbol{\varepsilon}^*=\left\{\begin{array}{c}\boldsymbol{\kappa}\\ \boldsymbol{\gamma}\end{array}\right\},\quad \boldsymbol{D}=\left[\begin{array}{cc}\boldsymbol{D}_b & \boldsymbol{0}\\ \boldsymbol{0} & \boldsymbol{D}_s\end{array}\right],\quad \boldsymbol{C}=\left[\begin{array}{ccc}\rho t & 0 & 0\\ 0 & \rho I & 0\\ 0 & 0 & \rho I\end{array}\right].$$

The frequency dependent parameters $\tau_1=\tau_1(\omega)$ and $\tau_2=\tau_2(\omega)$ are local mesh parameters determined from dispersion analysis and designed to improve the accuracy of the finite element solution (Thompson, 1999). Setting $\tau_1=\tau_2=0$, reverts to the underlying Hybrid formulation. The use of residuals maintains the consistency of the resulting finite element variational equation. Integration of the residuals over element interiors $\tilde{\Gamma}$ is required to maintain C^0 continuity between adjacent elements.

Using a mixed/hybrid finite element approach, independent approximations are used for the displacement variables and stress resultants – a compatible displacement field and a stress field defined in the interior of the element: $\boldsymbol{u}^*=\boldsymbol{N}\boldsymbol{d}$, $\boldsymbol{\sigma}^*=\boldsymbol{P}\boldsymbol{\beta}$, where $\boldsymbol{N}$ and $\boldsymbol{P}$ are arrays of polynomial basis functions and $\boldsymbol{d}$ and $\boldsymbol{\beta}$ are the unknown element nodal degrees-of-freedom (dof) and stress parameters, respectively. Any of several existing mixed finite element approximation fields which produce elements which are free from shear locking and pass the static patch test may be used. In (Thompson, 1999) we used the assumed displacement and stress fields proposed by Aminpour (Aminpour, 1992) to develop a 4-node Hybrid Least Squares (HLS) quadrilateral plate element. The transverse displacement interpolation is bi-linear in the nodal parameters w_i, enriched with linked quadratic functions expressed in terms of the nodal rotations θ_{xi} and θ_{yi}. The transverse displacement is approximated by polynomials of one order higher than the rotations, as a result, the shape functions are constructed to have a constant curvature and transverse shear along each side of the element, so that the element is automatically free from shear locking. The assumed moment and shear force fields are formulated in element natural coordinates and then transformed into physical coordinates by means of the contravariant tensor transformation evaluated at the center of the element. The shear resultant field is assumed *a priori* to satisfy the static equilibrium equations defined in natural coordinates,

Imposing stationary conditions with respect to $\boldsymbol{u}^*$ and $\boldsymbol{\sigma}^*$, and eliminating $\boldsymbol{\beta}$ from the resulting discrete Euler-Lagrange equations results in the dynamic stiffness matrix for each element:

$$\boldsymbol{s}^e=\boldsymbol{k}^e-\omega^2\boldsymbol{m}^e+\boldsymbol{k}^e_{LS} \tag{14}$$

composed of the element stiffness and mass matrices,

$$\boldsymbol{k}^e=\boldsymbol{T}^T\boldsymbol{H}^{-1}\boldsymbol{T},\qquad \boldsymbol{m}^e=\int_{\Gamma_e}\boldsymbol{N}^T\boldsymbol{C}\boldsymbol{N}\,d\Gamma \tag{15}$$

and the frequency dependent, generalized least-squares contribution $\boldsymbol{k}^e_{LS}=\boldsymbol{k}^e_{LS}(\omega)$. The stiffness matrix is computed from the arrays,

$$\boldsymbol{T}=\int_{\Gamma_e}\boldsymbol{P}^T\boldsymbol{B}\,d\Gamma,\qquad \boldsymbol{H}=\int_{\Gamma_e}\boldsymbol{P}^T\boldsymbol{D}^{-1}\boldsymbol{P}\,d\Gamma \tag{16}$$

For general 4-node quadrilateral finite elements with the stress and displacement fields defined by (Aminpour, 1992), the

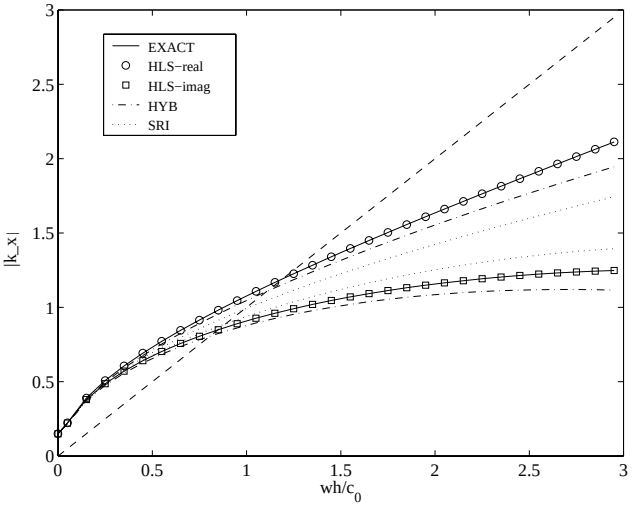

Figure 1. Comparison of analytic and finite element dispersion curves for steel plate *in vacuo* with $h/t = 1.0$. Real and Imaginary wavenumber pairs for Hybrid Least Squares (HLS), Hybrid (HYB), and Galerkin with Selectively Reduced Integration (SRI).

stabilization matrix $\boldsymbol{k}^e_{LS}$ is determined from a square element with length h and constant element jacobian $J^e = \frac{h^2}{4}$, i.e.,

$$\boldsymbol{k}^e_{LS} = r_1 \int_{-1}^{1}\int_{-1}^{1} \left(\frac{d\boldsymbol{N}_w^T}{d\xi}\frac{d\boldsymbol{N}_w}{d\xi} + \frac{d\boldsymbol{N}_w^T}{d\eta}\frac{d\boldsymbol{N}_w}{d\eta} \right) d\xi d\eta + r_2 \int_{-1}^{1}\int_{-1}^{1} \left(\frac{d\boldsymbol{N}_{\theta_x}^T}{d\xi}\frac{d\boldsymbol{N}_{\theta_x}}{d\xi} + \frac{d\boldsymbol{N}_{\theta_y}^T}{d\eta}\frac{d\boldsymbol{N}_{\theta_y}}{d\eta} \right) d\xi d\eta \quad (17)$$

where $\boldsymbol{N}_w(\xi,\eta)$, $\boldsymbol{N}_{\theta_x}(\xi,eta)$ and $\boldsymbol{N}_{\theta_y}(\xi,\eta)$ are row vectors of polynomial basis functions defined by finite element approximations in natural coordinates (ξ,η): $w = \boldsymbol{N}_w\boldsymbol{d}^e$, $\theta_x = \boldsymbol{N}_{\theta_x}\boldsymbol{d}^e$, , $\theta_y = \boldsymbol{N}_{\theta_x}\boldsymbol{d}^e$. The scaled mesh parameters $r_1 = \tau_1(m\omega^2)^2$ and $r_2 = \tau_2(\rho I\omega)^2$ are defined based on an average element length h. In (Thompson, 1999), optimal values for r_1 and r_2 are determined such that finite element wavenumber pairs $\pm k_1$ and $\pm k_2$ match the analytical wavenumber pairs for a given wave orientation angle φ on a uniform mesh.

Figure 1 shows a comparison of finite element and analytical dispersion curves for the propagating and evanescent wave numbers for a steel plate *in vacuo*. Results are given for a uniform mesh with waves directed along mesh lines. The dispersion curves are compared for elements based on standard Galerkin methods with Selective-Reduced Integration (SRI), the Hybrid element (HYB) of (Aminpour, 1992), and the Hybrid-Least-Squares element (HLS), (Thompson, 1999). The properties for the plate are taken as: $E = 210\times10^{10}$ dynes/cm^2, $\nu = 0.29$, $\rho = 7.8$ g/cm^2, and $\kappa = 5/6$. The ratio of the element length to plate thickness is $h/t = 1.0$. For reference, the frequency is normalized with respect to the element length h, and the speed of sound in water, $c_0 = 148100$ cm/s. The diagonal dashed line shows the sonic wavenumber $k_0 = \omega/c_0$. The *coincident frequency* for the fluid-loaded plate is located at the intersection where the in vacuo wavenumber for the plate k_1 matches the sonic wavenumber k_0. The SRI element under-estimates the propagating real wavenumber pair while overestimating the imaginary wavenumber. The HYB element matches the analytical propagating wavenumber much better, suggesting significant improvement in phase accuracy. The HLS element matches the analytical dispersion curves exactly by design.

COUPLED ACOUSTIC FLUID - PLATE EQUATIONS

For the fluid loaded plate, the acoustic pressure $p(x,y,z)$ appears as a surface traction in the vertical equation of motion for the plate:

$$Q_{x,x} + Q_{y,y} - m\omega^2 w(x,y) = q(x,y) - p(x,y,0), \quad (x,y)\in\Gamma \quad (18)$$

The fluid domain Ω_f is defined by the semi-infinite region $z \geq 0$. The bottom of the plate is assumed to be *in vacuo*. The acoustic pressure satisfies the Helmholtz equation,

$$(\nabla^2 + k_0^2)p(x,y,z) = 0, \qquad (x,y,z)\in\Omega_f \quad (19)$$

where $k_0 = \omega/c_0$, and $c_0 = K/\rho_0$ is the acoustic wave speed. To ensure outgoing waves, the acoustic pressure is also subject to the Sommerfeld radiation condition at infinity. The continuity of normal acceleration on the wet surface $z = 0$, is expressed as the Neumann condition,

$$\left.\frac{\partial p}{\partial z}\right|_{z=0} = \rho_0\omega^2 w(x,y), \qquad \text{on } \Gamma \quad (20)$$

Assume free plane waves propagating in the x-direction within the fluid-loaded plate with no sources $q = 0$. The plate vertical deflection w and rotation $\theta = \theta_x$ is sought in the following form:

$$w = w_0 e^{ik_x x}, \qquad \theta = \theta_0 e^{ik_x x} \quad (21)$$

Then, the acoustic pressure field satisfies the boundary condition,

$$\left.\frac{\partial p}{\partial z}\right|_{z=0} = \rho_0\omega^2 w_0 e^{ik_x x} \quad (22)$$

With these conditions, the functions w, θ, and p are independent of y, so that the governing equations can be simplified to,

$$Q_{x,x} - m\omega^2 w(x) = -\,p(x,z)|_{z=0} \quad (23)$$

$$M_{x,x} - Q_x + \rho I\omega^2\theta(x) = 0 \quad (24)$$

Eliminating θ in favor of w gives the single equation:

$$w_{,xxxx} + \lambda_s^2 w_{,xx} - \lambda_b^4 w = -\frac{1}{D_s}\left[F_1 p + p_{,xx}\right]\big|_{z=0} \qquad (25)$$

with frequency dependent functions, $\lambda_s^2 = [k_p^2 - k_s^2]$, $\lambda_b^4 = [k_p^2 k_s^2 + k_b^4/D_s]$, $F_1 = [k_p^2 + 1/D_b]$. Here, $k_p = (\rho I/D_b)^{1/2}\omega$, $k_s = (m/D_s)^{1/2}\omega$, and $k_b = (m\omega^2/D_b)^{1/4}$ is the classical plate bending wavenumber for *in vacuo* flexural waves in the Kirchoff theory.

Assuming a plane wave solution for acoustic pressure:

$$p(x,z) = p_0 e^{i(k_x x + k_z z)} \qquad (26)$$

then to satisfy (22) and (19),

$$p(x,z) = \frac{\rho_0 \omega^2}{i k_z} w_0 e^{i(k_x x + k_z z)} \qquad (27)$$

with k_z defined by,

$$k_0^2 = k_x^2 + k_z^2. \qquad (28)$$

The dispersion equation for the fluid-loaded plate is obtained by introducing (21) and (27) into the plate equation (25), with the result:

$$D(k_x) = i k_z D_s (k_x^4 - \lambda_s^2 k_x^2 - \lambda_b^4) + \rho_0 \omega^2 (F_1 - k_x^2) = 0 \qquad (29)$$

The roots of this equation give the possible wavenumbers k_x and k_z of the free plane waves. Squaring both sides of (29) and using (28) to eliminate k_z in terms of k_x, the dispersion equation can be replaced by,

$$D_s^2 (k_0^2 - k_x^2)(k_x^4 - \lambda_s^2 k_x^2 - \lambda_b^4)^2 - \rho_0^2 \omega^4 (F_1 - k_x^2)^2 = 0 \qquad (30)$$

Considered as an equation in k_x^2, the dispersion equation has five roots. The absolute value for the real and imaginary parts of the k_x roots are plotted in Figure 2 using the fluid-loaded plate properties given earlier, and with fluid density $\rho_0 = 1.0\text{g/ cm}^3$. The components k_z are computed from (28) and plotted in Figure 3. There is one real k_x root over all frequencies with modulus larger than the acoustic wavenumber k_0. Since $k_x > k_0$, this root is interpreted as a *subsonic* free-wave. For frequencies above the cutoff frequency, the subsonic wavenumber asymptotes to the the sonic line $k_0 = \omega/c_0$. For this root, $k_z^2 = k_0^2 - k_x^2 < 0$, so that the component $k_z = i\sqrt{k_x^2 - k_0^2}$ is purely imaginary, and the pressure decreases exponentially with respect to the variable z. The energy associated with this wave is trapped in the acoustic near-field of the plate. The leaky wavenumbers are characterized by the roots where the imaginary part of k_x is much smaller than the real part, i.e., $\text{Re}(k_x) \gg \text{Im}(k_x)$. In the region $k_0 < k_1$, the k_x component of the leaky wavenumbers initially occur as complex conjugate pairs and then quickly bifurcate into two paths of pure real roots such that $k_0 < k_x < k_1$. As the frequency increases, the paths rejoin to form a complex conjugate pair. The evanescent wavenumbers occur as complex conjugate pairs over the entire frequency range, with $\text{Im}(k_x) \gg \text{Re}(k_x)$.

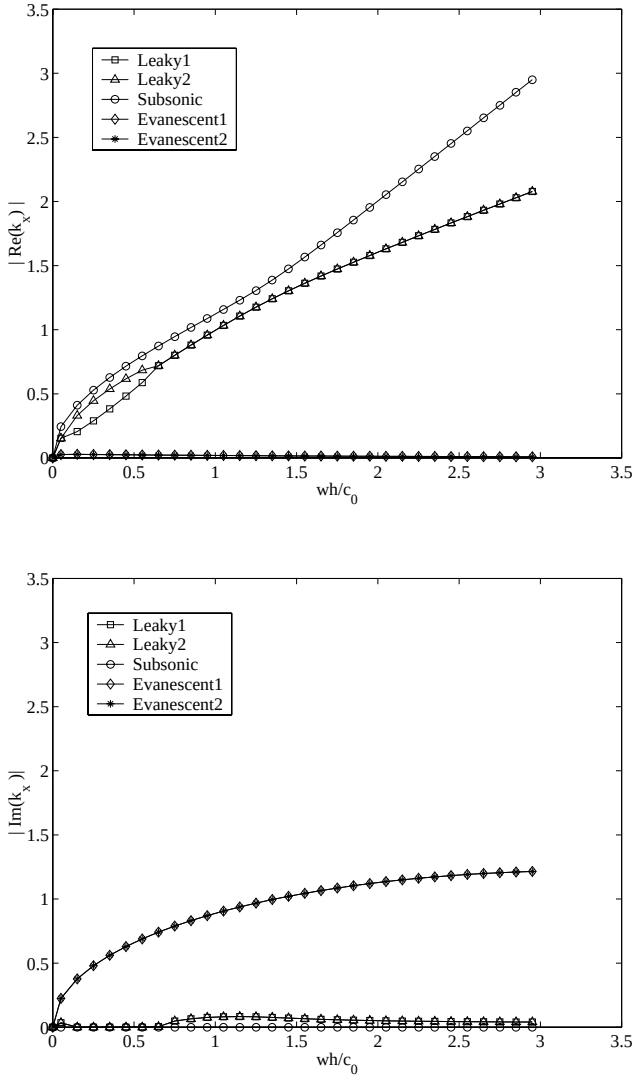

Figure 2. Analytical dispersion relations for roots k_x. (Top) Real Part, (Bottom) Imaginary Part.

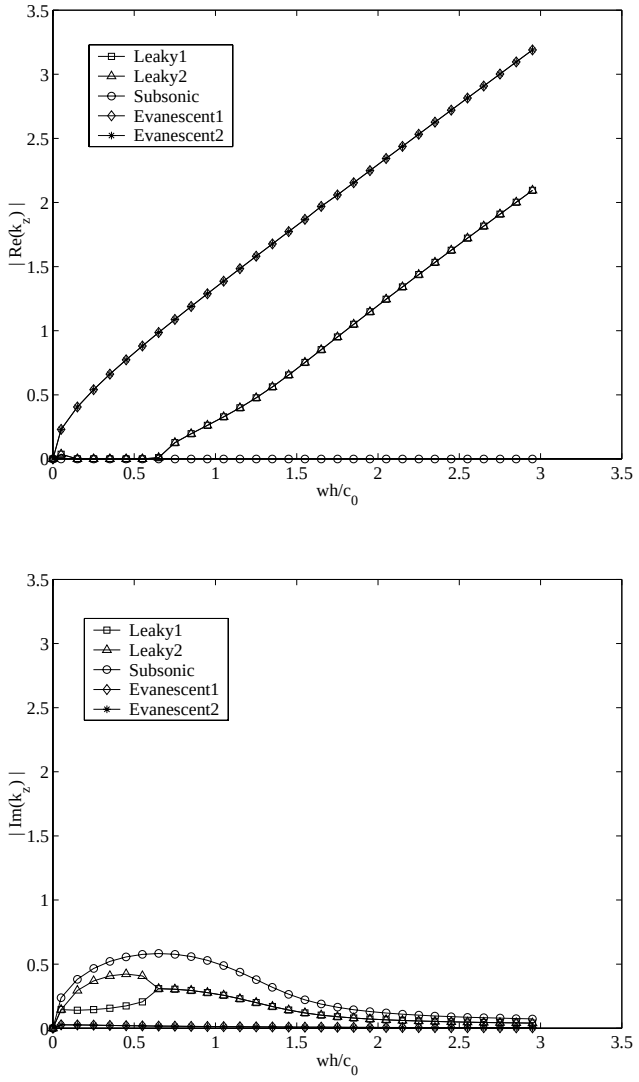

Figure 3. Analytical dispersion relations for roots k_z. (Top) Real Part, (Bottom) Imaginary Part.

FINITE ELEMENT FORMULATION

The variational equation for the coupled fluid-structure problem is,

$$\delta\left(\Pi_s + \Pi_f\right) = \delta W \tag{31}$$

where the structural part $\Pi_s = \Pi_{HLS}(\boldsymbol{u}^*, \boldsymbol{\sigma}^*)$ is the Hybrid-Least-Squares functional defined earlier for the plate, and the fluid part $\Pi_f = \Pi_{GLS}(p)$ is defined by a Galerkin functional modified by a least-squares term:

$$\Pi_{GLS}(p) = \Pi_G(p) + \frac{1}{2}\int_{\tilde{\Omega}_f} \tau(\nabla^2 p + k_0^2)^2 d\Omega \tag{32}$$

$$\Pi_G(p) = \frac{1}{2}\int_{\Omega_f} (\nabla p)^2 d\Omega + \frac{1}{2}k_0^2 \int_{\Omega_f} p^2 d\Omega \tag{33}$$

The right-hand-side is the 'virtual work' given by,

$$\delta W = \int_\Gamma \delta w\,(q-p) d\Gamma - \rho_0\omega^2 \int_\Gamma \delta p\, w d\Gamma \tag{34}$$

In the above, τ is the optimal GLS design parameter for the uncoupled acoustic fluid problem given in (Thompson, 1995). For $\tau = 0$ the formulation reverts to Galerkin. Introducing finite element approximations for the acoustic pressure $p = \boldsymbol{\psi}\boldsymbol{p}$, together with the displacement and stress approximations for the plate discussed earlier, and imposing stationary conditions with respect to p, and $(\boldsymbol{u}^*, \boldsymbol{\sigma}^*)$, leads to the coupled system of equations for fluid-loaded plate elements,

$$\begin{bmatrix} \boldsymbol{s}^e & \boldsymbol{q}^e \\ \boldsymbol{q}^{eT} & \boldsymbol{h}^e \end{bmatrix} \begin{Bmatrix} \boldsymbol{d}^e \\ \boldsymbol{p}^e \end{Bmatrix} = \begin{Bmatrix} \boldsymbol{f}^e \\ 0 \end{Bmatrix} \tag{35}$$

where $\boldsymbol{h}^e = (\boldsymbol{k}^f - k_0^2 \boldsymbol{m}^f + \boldsymbol{k}^f_{LS})/(\rho_0\omega^2)$, is the fluid dynamic stiffness matrix composed of standard fluid stiffness and mass matrices and a least-squares stabilization matrix described in (Thompson, 1995). The matrix $\boldsymbol{q}^e$ defines the coupling matrix resulting from (34). For waves restricted to the *xz*-plane it is sufficient to consider two-dimensional 4-node bilinear acoustic elements. In this case, the optimal τ for the uncoupled fluid is given by (Thompson, 1995):

$$\tau k_0^2 = 1 - \frac{6(4 - f_x - f_z - 2f_x f_z)}{(k_0 h)^2 (2+f_x)(2+f_z)} \tag{36}$$

where $f_x = \cos(k_0 h \cos\pi/8)$, $f_z = \cos(k_0 h \sin\pi/8)$, and $k_0 = \omega/c_0$.

FINITE ELEMENT DISPERSION ANALYSIS

Finite element dispersion relations for the fluid-loaded plate are obtained by assembling a patch of elements from a uniform mesh with grid spacing $\Delta x = \Delta z = h$, (Jasti, 1992; Grosh, 1994). The result is three repetitive stencils associated with solutions $\boldsymbol{v}_n = [w_n\,,\, \theta_n\,,\, p_{n,0}\,,\, p_{n,1}]^T$, at a typical node n:

$$\sum_{l=-1}^{1} \boldsymbol{B}_l \boldsymbol{v}_{n+l} = 0 \tag{37}$$

Here $\boldsymbol{B}_l$ are (3×4) matrix partitions which depend on frequency and the element dynamic stiffness coefficients. The notation $p_{n,0}$ denotes pressure solutions at a node lying on the plate boundary

at $z = 0$, while $p_{n,1}$ denotes solutions at a typical node along the first row of grid points in the fluid defined by $z = h$.

Wave solutions in the plate are assumed to be directed in the x-direction,

$$\left\{ \begin{array}{c} w_n \\ \theta_n \end{array} \right\} = \left\{ \begin{array}{c} w_0 \\ \theta_0 \end{array} \right\} \mathrm{e}^{(ik_x nh)} \tag{38}$$

while the pressure solutions take exponential form in the xz-plane,

$$p_{n,m} = p_0 \mathrm{e}^{(ik_x nh)} \, \mathrm{e}^{(ik_z nh)} \tag{39}$$

The dispersion relations for the fluid-loaded plate are obtained by substituting (38) and (39) into the stencils (37) and using the GLS dispersion relation for the uncoupled fluid relating wavenumber components k_x and k_z, to frequency $k_0 = \omega/c_0$ given by (Thompson, 1995): $g_2 c_z + g_1 = 0$, where $g_2 = (c_x h_{13} + h_{14})$, $g_1 = (c_x h_{12} + h_{11})$, and $c_x = \cos(k_x h)$, and $c_z = \cos(k_z h)$, and $s_x = \sin(k_x h)$.

The result are the coupled relations,

$$\left[\begin{array}{ccc} S_{11} & -iS_{12} & Q_1 \\ iS_{12} & S_{22} & -iQ_2 \\ Q_1 & iQ_2 & H_1 \end{array} \right] \left\{ \begin{array}{c} w_0 \\ \theta_0 \\ p_0 \end{array} \right\} = \left\{ \begin{array}{c} 0 \\ 0 \\ 0 \end{array} \right\} \tag{40}$$

with the Fourier transform of the difference operator associated with: the plate equations, $S_{11} = s_{13} c_x + s_{11}$, $S_{22} = s_{24} c_x + s_{22}$, $S_{12} = s_{23} s_x$; the coupling equations, $Q_1 = q_{12} c_x + q_{11}$ $Q_2 = q_{41} c_x$; and fluid equations, $H_1 = \pm\sqrt{g_1^2 - g_2^2}/(\rho_0 \omega^2)$. Here $s_{ij} = [\boldsymbol{s}^e]_{ij}$, $h_{ij} = [\boldsymbol{h}^e]_{ij}$, and $q_{ij} = [\boldsymbol{q}^e]_{ij}$, are coefficients of the element dynamic stiffness arrays. The fluid-loaded plate dispersion relation is obtained by rooting the characteristic polynomial obtained from the determinant of (40).

Figure 4 (Top) shows the relative dispersion error in the subsonic finite element wavenumber k_x^h divided by the analytic wavenumber k_x. This real wavenumber component corresponding to propagating waves, often plays a dominant role in fluid-loaded plates. Thus by reducing the percent error in the real wavenumber, even if by a small amount, the overall accuracy of the numerical solution can increase significantly. The results show that the SRI plate element with a Galerkin approximation for the fluid (SRI-Gal) gives very large errors, both below and above the coincident frequency. In contrast, the Hybrid plate element with Galerkin Least-Squares approximation for the fluid (HYB-GLS) reduces the error significantly. The Hybrid Least-Squares plate element together with GLS for the fluid (HLS-GLS) improves the accuracy even further, closely matching the analytical wavenumber. The Galerkin Gradient-Least-Squares (GGLS) plate element developed in (Grosh, 1996), coupled with

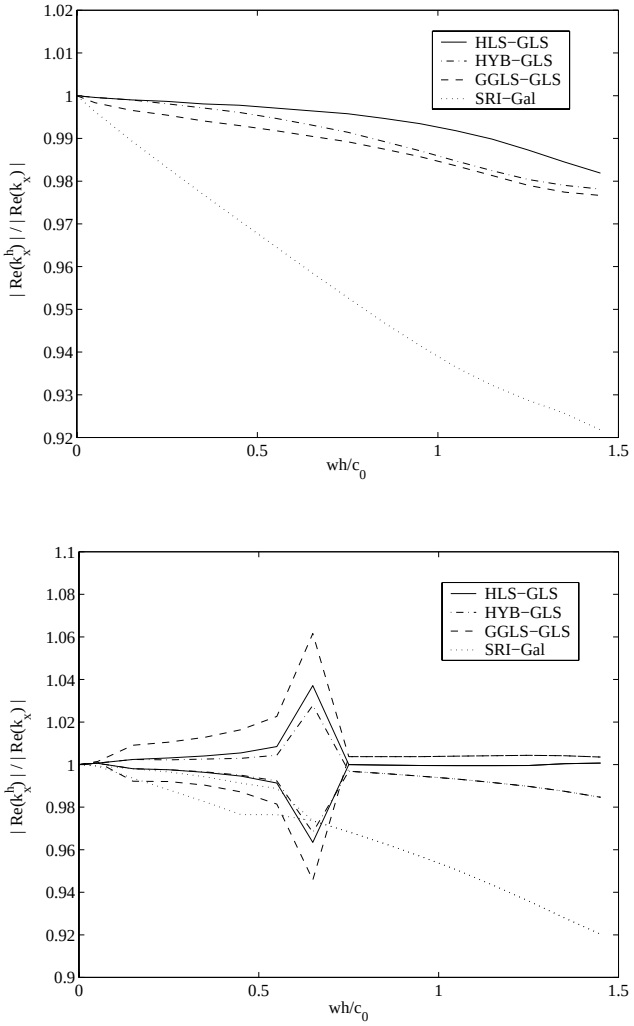

Figure 4. Relative error for real part of wavenumber k_x with $h/t = 1$. (Top) Subsonic, (Bottom) Leaky.

GLS fluid elements with the τ given in (36) is also compared. We note that this GGLS plate element is restricted to rectangular elements only. Below coincidence, GGLS-GLS shows significant error and then approaches the HYB-GLS solution for frequencies higher than coincidence.

Figure 4 (Bottom) shows the relative dispersion error in the real part of the leaky wavenumber k_x. In the bifurcation region, the HYB-GLS solution matches the analytical wavenumber closely. However, after rejoining to form a pair of complex conjugate roots, HYB-GLS under-estimates the analytical wavenumbers. The HLS-GLS solution matches the analytical leaky component over the entire frequency range. The spike in the error near $\omega h/c_0 = 0.6$ is a result of missing the bifurcation point by a small amount. Similar to the subsonic wavenumber results, the leaky wavenumber solutions for GGLS-GLS show significant error prior to coincidence. The solution using SRI

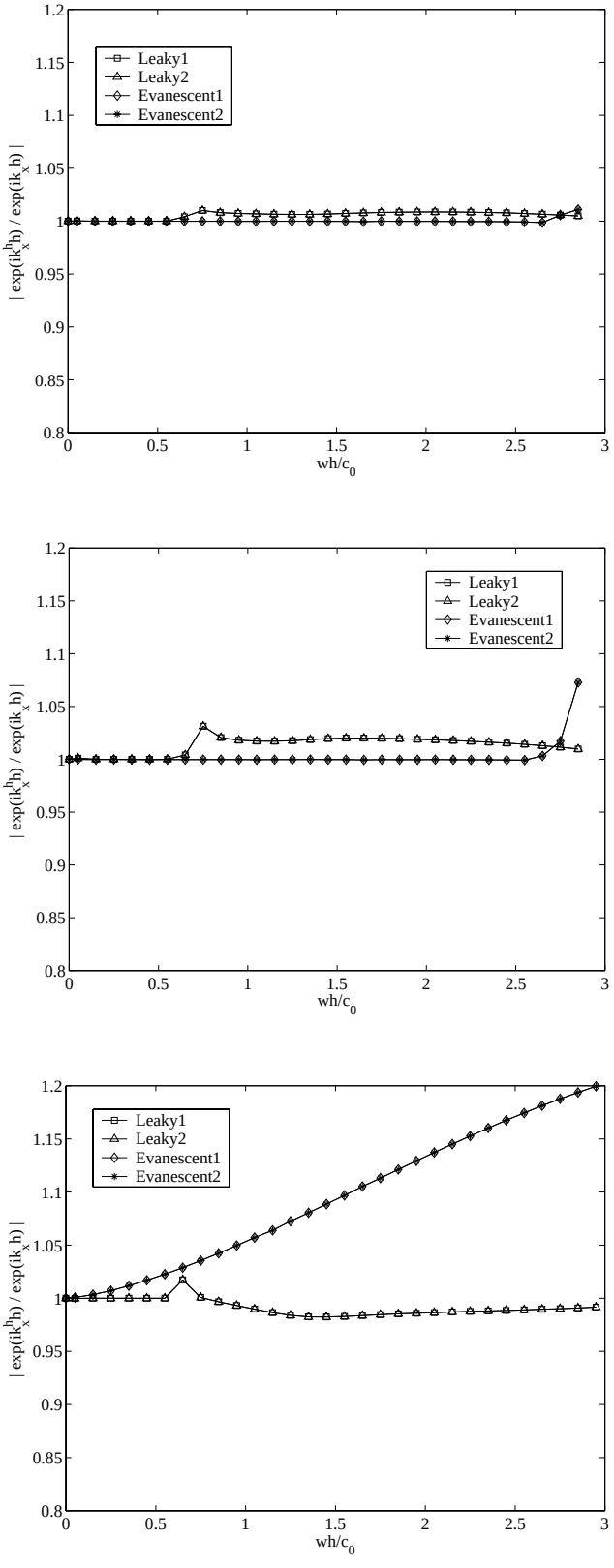

Figure 5. Relative error for imaginary part of wavenumber k_x with $h/t = 1$. (a) HYB-GLS, (b) GGLS-GLS, (c) SRI-Gal.

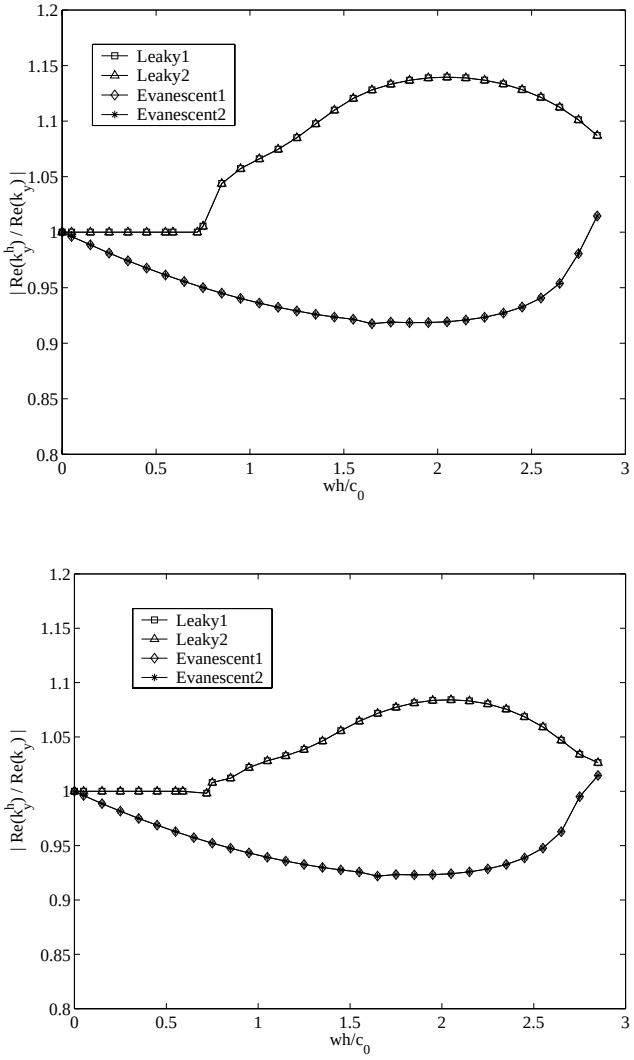

Figure 6. Relative error for real part of wavenumber k_y with $h/t = 1$. (a) HYB-GLS, (b) GGLS-GLS.

completely misrepresents the leaky wavenumbers both in the bifurcation and complex conjugate regions.

Figure 5 shows the relative error for $\mathrm{Im}(k_x)$. Results show significant error in the evanescent wavenumber using SRI-Gal. In contrast, both HLS-GLS and GGLS-GLS evanescent wavenumbers match the analytical value over the entire range of frequencies. The similarities in the evanescent wavenumbers is explained by the dominant influence of the common GLS treatment for the fluid region. The error in the leaky wavenumber is largest for the GGLS-GLS method. The relative error of $\mathrm{Re}(k_y)$, producing propagating waves in the fluid are shown in Figure 6. Evanescent solutions for HYB-GLS and GGLS-GLS are very similar, again showing the significance of the common GLS fluid treatment. The phase error in the k_y component of leaky wavenumbers is slightly smaller using the GGLS-GLS method.

CONCLUSIONS

A complex-wavenumber dispersion analysis of fluid-loaded Reissner-Mindlin plates based on the hybrid least squares method (HLS) developed in (Thompson, 1999) is performed. Through judicious selection of the design parameters inherent in the least-squares modification, this formulation provides a consistent framework for enhancing the accuracy of mixed Reissner-Mindlin plate elements. Improvement in accuracy for the fluid-loaded plate is provided by the GLS method (Thompson, 1995) applied to the acoustic fluid region. The least-squares modifications are simple to implement with negligible increase in computational cost and memory. We note that high-order accuracy may also be achieved by 'brute-force' using higher-order finite element approximations such as p-version or spectral extensions (Thompson, 1993), but with substantial extra cost and memory requirements.

Dispersion analysis provides a tool for comparing the free-waves in different finite element formulations for fluid-loaded plates. The analysis of free-waves in an infinite mesh allows us to predict the trends in behaviour of the elements when used to model boundary value problems with fixed boundaries. Results from our finite element dispersion relations demonstrate the improved accuracy of the hybrid least-squares (HLS) plate element together with the GLS fluid treatment, compared to the underlying hybrid (HYB) element (Aminpour, 1992), and standard displacement-based elements based on selectively reduced integration (SRI). Results show that the SRI plate element coupled with a Galerkin fluid approximation performs poorly for both subsonic, evanescent, and leaky wavenumber components. The accuracy of the assumed-stress hybrid element (HYB), coupled with a GLS fluid treatment, is dramatically improved compared to SRI and performs well. Using the least-squares modification for the hybrid plate (HLS), together with GLS fluid elements, the performance of the hybrid element is enchanced further, yielding a highly accurate fluid-loaded plate model.

In general, the ability to accurately represent all wavenumber components is important. However, for many classes of problems, the subsonic wavenumber plays a dominant role. The HLS approach has a lower error than the GGLS approach for the important subsonic wavenumber. The error for HLS is lower than GGLS for the k_x leaky wavenumber component, yet higher for the k_y leaky wavenumber. Both HLS and GGLS give similar results for evanescent wavenumbers. Further research is needed to determine the relative importance of the finite element wavenumbers when boundary conditions are included in the analysis.

ACKNOWLEDGMENT

Support for this work was provided by the National Science Foundation under Grant CMS-9702082 in conjunction with a Presidential Early Career Award for Scientists and Engineers (PECASE), and is gratefully acknowledged.

REFERENCES

L.L. Thompson and Y. Tong, 'Hybrid Least Squares Finite Element Methods for Reissner-Mindlin Plates', *Proceedings of the ASME Noise Control and Acoustics Division – 1999*, 1999 ASME International Mechanical Engineering Congress and Exposition, Symposium on Innovative Experimental and Numerical Techniques for Structural Vibration and Acoustics Problems, ASME, NCA-Vol.26, (1999), 77-89.

L.L. Thompson, and P.M. Pinsky, 'A Galerkin least squares finite element method for the two-dimensional Helmholtz equation', *Internat. J. Numer. Methods Engrg.* **38**, (1995) 371-397.

T.J.R. Hughes, L.P. Franca, and G.M. Hulbert, 'A new finite element formulation for computational fluid dynamics: VIII. The Galerkin least squares method for advective-diffusive equations', *Comp. Meth. in Appl. Mech. Eng.*, **73** (1989), 173-189.

I. Harari and T.J.R. Hughes, 'Galerkin/least-squares finite element methods for the reduced wave equation with non-reflecting boundary conditions in unbounded domains', *Comp. Meth. in Appl. Mech. Eng.*, 98 (1992), 411-454.

I. Harari, K. Grosh, T.J.R. Hughes, M. Malhotra, P.M. Pinsky, J.R. Stewart, L.L. Thompson, 'Recent Developments in Finite Element Methods for Structural Acoustics', *Archives of Computational Methods in Engineering*, **3**, pp. 132-311, 1996.

T.J.R. Hughes and L.P. Franca, 'A mixed finite element method formulation for Reissner-Mindlin plate theory: uniform convergence of all higher-order spaces', *Comput. Meths. Appl. Mech. Engrg.*, 67 (1988), 223-240.

K. Grosh and P.M. Pinsky, 'Galerkin Generalized Least Squares Methods for Timoshenko Beams', *Comp. Meth. in Appl. Mech. Eng.*, 132 (1996) 1-16.

L. P. Franca and D. G. Dutra do Carmo, 'The Galerkin gradient least-squares method', *Comput. Meths. Appl. Mech. Engrg.*, 74 (1989), 44-54.

K. Grosh and P.M. Pinsky, 'Galerkin Generalized Least Squares Methods for time-harmonic structural acoustics', *Comp. Meth. in Appl. Mech. Eng.*, 154 (1998) 299-318.

R. Jasti, 'Mixed shell finite elements with applications in structural acoustics', Chapter 8, PhD dissertation, Stanford University, 1992.

K. Grosh and P.M. Pinsky, 'Complex wave-number dispersion analysis of Galerkin and Galerkin least-squares methods for fluid-loaded plates', *Comp. Meth. in Appl. Mech. Eng.*, 113 (1994) 67-98.

M.A. Aminpour, 'An assumed-stress Hybrid 4-node shell element with drilling degrees of freedom', *Internat. J. Numer. Methods Engrg.* **33**, (1992) 19-38.

L.L. Thompson and P.M. Pinsky, 'Complex wavenumber Fourier analysis of the p-version finite element method', *Computational Mechanics*, Vol. 13, No. 4 (1994), 255-275.